의학석사 학위논문

가도세틱산 조영증강 MRI 에서의 국소 간 병변의 크기 측정과 LI-RADS 분류에 대한 영향

Size measurement of focal hepatic observations on gadoxetate disodium-enhanced MRI and its impact on LI-RADS classification

울산대학교대학원

의 학 과

최 지 영

가도세틱산 조영증강 MRI 에서의 국소 간 병변의 크기 측정과 LI-RADS 분류에 대한 영향

지도교수 최 상 현

이 논문을 의학석사 학위 논문으로 제출함

2022 년 2 월

울산대학교대학원

의 학 과

최 지 영

최지영의 의학석사학위 논문을 인준함

심사위원 김 경 원 (인)

심사위원 김 소 연 (인)

심사위원 최 상 현 (인)

울산대학교대학원

2022 년 2 월

Abstract

Purpose: We aimed to determine the optimal image sequence for measurement of hepatic observations on gadoxetate disodium-enhanced MRI in comparison with pathologic measurement, and to evaluate its clinical impact on the Liver Imaging Reporting and Data System (LI-RADS) v2018 classification.

Materials and Methods: Two hundred and fifty-three patients (279 hepatic observations) who underwent gadoxetate disodium-enhanced MRI and subsequent hepatectomy were retrospectively included. Two radiologists independently evaluated the visualization score (five-point scale) and size of each observation on six MRI sequences (T1-weighted, T2-weighted, arterial-phase, portal venous-phase, transitional-phase [TP], and hepatobiliary-phase [HBP] images) and assigned a LI-RADS category. Correlations between MRI and pathologic measurements were evaluated using Pearson correlation coefficients. A repeated measures analysis of variance with Bonferroni post-hoc comparison tests was used to compare the visualization scores and absolute differences between MRI sequences and pathologic measurements. The LI-RADS classification according the size measurement of each MRI sequence was compared using Cochran's Q test with a post-hoc McNemar's test.

Results: The 279 observations included 247 hepatocellular carcinomas (HCC), 21 non-HCC malignancies, and 11 benignities. Of the MRI sequences, HBP had the highest visualization score (4.1 ± 0.6) and correlation coefficient (r = 0.965). The absolute difference between MRI and pathologic measurement was lowest on TP (2.3 mm ± 2.2), followed by HBP (2.4 mm ± 2.1). In the LI-RADS classifications, HBP had no LI-RADS category noncategorizable (LR-NC).

Conclusion: Hepatobiliary-phase images are clinically useful for measuring hepatic observations on gadoxetate disodium-enhanced MRI, especially regarding visibility, correlation with pathologic findings, and LI-RADS classification.

차례

표 및 그림목차

Introduction

Hepatocellular carcinoma (HCC) is the most common primary hepatic malignant tumor and the fourth most common cause of cancer-related death worldwide (1, 2). Because the diagnosis of HCC can be noninvasively made on the basis of specific imaging features without pathologic confirmation (3, 4), the accurate imaging diagnosis of HCC is an important clinical issue in the management of patients at risk for HCC. To improve the performance and standardization of the imaging diagnosis of HCC in at-risk patients, the Liver Imaging Reporting and Data System (LI-RADS) was developed in 2011 (5), and fully integrated into the American Association for the Study of Liver Diseases (AASLD) 2018 HCC clinical practice guidance (6). LI-RADS assigns categories to liver observations (i.e., LR-1 to LR-5) on the basis of the presence of major and ancillary imaging features, with the major features including observation size, nonrim arterial-phase hyperenhancement, nonperipheral washout, enhancing capsule, and threshold growth.

Out of the five major features, two items (observation size and threshold growth) are related to the size of observation. Because the probability of HCC in a cirrhosis-associated nodule is positively correlated with the size of the observation (i.e., observations <2.0 cm are more likely to be benign or well-differentiated malignancy, whereas the likelihood of malignancy increases in larger observations) (7, 8), observation size is considered an important major feature. In addition, treatment allocation of patients with hepatocellular carcinoma is dependent on lesion size. Thus, the accurate size measurement of observations is essential for providing proper management. Although LI-RADS states that size measurement should not be performed in arterial-phase (AP) or diffusion-weighted image (DWI) (6), there is a lack of clear guidance on which image sequence is optimal for size measurement.

A few studies have investigated correlations in HCC size between pathologic measurements and those on CT and MRI (9, 10), the results of these previous studies were limited because they did not provide results according to the specific phase of imaging (9), and also exclusively included HCC without including benign lesions or non-HCC malignancies (10). In addition, gadoxetate disodium contrast agent has different pharmacokinetic characteristics to other extracellular contrast agents, and the evidence as to which image sequence is the most suitable for size measurement on gadoxetate disodium-enhanced MRI is insufficient.

Therefore, we aimed to determine the optimal image sequence for gadoxetate disodium-enhanced MRI in terms of size measurement of hepatic observations in comparison with pathologic measurement, and to evaluate its clinical impact on the LI-RADS v2018 classification.

Materials and Methods

This study was approved by the institutional review board of our center, which waived the need for informed patient consent because of the study's retrospective nature.

Patients

From our institution's computerized databases, 595 patients who underwent gadoxetate disodium-enhanced MRI and subsequent hepatectomy within 1 month between January 2017 and December 2017 (**Figure 1**) were retrospectively identified. Of these 595 patients, 157 were excluded because of no risk factor for HCC, 79 because of a hepatic observation more than 5 cm, 102 because they had undergone locoregional treatment for HCC before surgery, and four because of no focal lesion on pathology. Finally, 253 patients with 279 hepatic observations were analyzed in the present study.

MRI technique

MRI examinations were performed using 1.5-T (Magnetom Avanto; Siemens Healthineers, Erlangen, Germany) or 3.0-T (Magnetom Skyra, Siemens Healthineers) scanners. The MRI protocol consisted of non-enhanced MRI using breath-hold dual gradient-echo T1-weighted imaging (T1WI), respiratory-triggered turbo spin echo T2-weighted imaging (T2WI), DWI using a respiratory-triggered single-shot echo-planar imaging sequence with *b* values of 0, 50, 500, and 900 s/mm^2, and contrast-enhanced MRI. The contrast-enhanced MRI used a fat-suppressed three-dimensional spoiled gradient echo T1-weighted sequence. After intravenous injection of 0.1 mL/kg body weight of gadoxetate disodium at 1 mL/s followed by a 20 mL saline flush, the following four image sequences were obtained at different phases: AP (determined using a test-bolus method); portal venous-phase (PVP, 25 s after completion of the AP images); transitional-phase (TP, 3 minutes after contrast injection); and hepatobiliary-phase (HBP, 20 minutes after contrast injection). Further details of the MRI techniques and sequence parameters are provided in **Table 1**.

Image analysis

Images were independently reviewed by two abdominal radiologists (J.Y.C. and J.Y.H. with 4 and 2 years of experience in hepatic imaging, respectively). Because this study was mainly focused on the size measurement of hepatic observations, the readers were informed of the location of the target observations to be analyzed, but were blinded to the pathologically-measured size of the target observations. The list of target hepatic observations correlating with pathologic findings was prepared by the third investigator (S.H.C.) who was not involved in the image analysis.

The readers evaluated the visibility of hepatic observations on the following six MRI sequences, T1WI, T2WI, AP, PVP, TP, and HBP. The visibility of hepatic observations on each sequence was scored using a 5-point scale: 1=non-visible; 2=visible, but faint; 3=equivocal; 4=mostly clear

margin, but partly indistinct; and 5=perfectly demarcated margin. For visible hepatic observations, size measurement was performed using the largest outer-edge-to-outer-edge dimension on both axial and coronal reconstructed images of each sequence according to LI-RADS v2018 (6). The largest value in the three dimensions of axial and coronal images was determined as the size of the hepatic observations. In addition, the readers analyzed the presence or absence of major features (arterial-phase hyperenhancement, washout, or enhancing capsule), ancillary features, and targetoid mass features according to LI-RADS v2018 (6). LI-RADS category was assigned based on the observation size measured in each MRI sequence. When LI-RADS classification was not available because of invisibility of hepatic observation in the analyzed MRI sequence, we categorized it into noncategorizable (LR-NC), although LI-RADS suggests that an observation can be considered as LR-NC if it cannot be categorized because key phases were omitted or degraded.

In the case of any discrepancies between the two readers, the average value between the two readers was used for both visualization score and observation size, and re-evaluation with a third reader was made to reach a consensus on LI-RADS category assignment.

Reference standard

Gross liver specimens were thoroughly examined and evaluated by experienced pathologists. The resected liver was regularly cut at 5 mm intervals to reveal the largest cross-section centered on the hepatic mass. The pathologists identified the hepatic mass in each sliced section and analyzed its characteristics including location, size, and resection margin. Mass size was expressed as a three-dimensional measurement of the longest axes (width×length×height). For each mass, at least three formalin-fixed paraffin-embedded blocks containing the tumor and adjacent non-neoplastic liver tissue were fabricated, and all hematoxylin-eosin-stained slides were reviewed by expert hepatobiliary pathologists. If necessary, immunohistochemical staining was performed to determine the final diagnosis.

Statistical Analysis

Continuous data are expressed as mean and standard deviation, and proportions as number and percentage. Statistical analysis was performed using SPSS Statistics for Windows version 23.0 (SPSS Inc., Chicago, IL, USA) and R version 4.0.3 (R Foundation for Statistical Computing, Vienna, Austria). For post-hoc pairwise comparison, we used Bonferroni correction method to adjust for multiplicity, and all p values were considered statistically significant at $p<.05$.

The visualization scores for the visibility of hepatic observations were compared between the six MRI sequences using repeated measures analysis of variance (RM ANOVA) with post-hoc comparison tests.

We compared the largest value in the three dimensions of MRI with the largest value in the three dimensions of pathologic specimen. To compare the observation size on the six MRI sequences with the size determined by pathologic evaluation, correlations between MRI and pathologic measurements were calculated using the Pearson correlation coefficient. The correlation coefficients (*r*) from these comparisons were interpreted as follows: 0.90–1.00=very strong correlation; 0.70–0.89=strong correlation; 0.40–0.69=moderate correlation; 0.10–0.39=weak correlation; 0.00–0.10=negligible correlation (11). In addition, an RM ANOVA with post-hoc comparison tests was used to compare MRI sequences in terms of the absolute difference between MRI and pathologic measurements, which was defined as the magnitude of the difference between the two measurements. Bland-Altman plots were also used to assess agreement between MRI and pathologic measurements.

To evaluate the clinical impact of size measurement using the different MRI acquisitions, the LI-RADS classification according to the size measurement of each MRI sequence was assessed, and compared between the six MRI sequences using a Cochran's Q test with post-hoc McNemar's test.

Inter-reader reliability in the visualization score and size measurement was evaluated using intraclass correlation coefficients (ICC): 0.00–0.40=poor; 0.40–0.59=fair; 0.60–0.74=good; and 0.75–1.00=excellent (12).

Results

Patient Characteristics

The clinical characteristics of the 253 included patients with 279 observations are summarized in **Table 2**. The patients included 187 men (mean age = 63 years; range = 39–83) and 66 women (mean age = 65 years; range = 43–84). Of the 253 patients, 114 (45.1%, 114/253) had liver cirrhosis. The most common risk factor was hepatitis B (80.2%, 203/254), followed by hepatitis C (8.3%, 21/254). The mean size of the 279 included observations on pathologic measurement was 26.4 ± 11.2 mm (range = 4.0–50.0 mm). Of the 279 observations, 247 were confirmed as HCC, 21 as non-HCC malignancy (11 cholangiocarcinomas, nine combined hepatocellular cholangiocarcinomas, and one metastasis), and 11 as benignity (five dysplastic nodules, three hemangiomas, two regenerative nodules, and one bile ductular proliferative lesion).

Visualization scores on the six MRI sequences

Of the six MRI sequences, HBP showed the highest visualization score (4.1 ± 0.6), which was significantly higher than that on the other five MRI sequences (all $p<.001$; **Table 3**). TP had the second-highest visualization score (3.6 ± 1.1), which was similar to that of T2WI, and both were significantly higher than the other three MRI sequences ($p\leq.001$). In the assessment of inter-reader reliability of

visualization score, HBP had the highest ICC (0.84, 95% confidence interval [0.80, 0.88]; **Table 4**).

Correlations between MRI and pathologic measurements

Table 5 summarizes the correlations and comparisons of absolute differences in observation size between pathologic assessment and each MRI sequence. Observation size on all six MRI sequences showed a very strong and statistically significant correlation (all p<.001 and r>0.9) with pathologic assessment. Of the six MRI sequences, HBP showed the highest correlation coefficient (r=0.965), followed by TP (r=0.960). The absolute difference between MRI and pathologic measurement was lowest on TP (2.3 mm ±2.2), followed by HBP (2.4 mm ±2.1), with no significant difference between TP and HBP (p>.999). Both TP and HBP had significantly lower absolute differences than AP (2.3 mm vs. 2.8 mm, p=.002 for TP; 2.4 mm vs. 2.8 mm, p=.002 for HBP) or PVP (2.3 mm vs. 2.7 mm, p=.006 for TP; 2.4 mm vs. 2.7 mm, p=.028 for HBP). Bland-Altman plots demonstrating the agreement between each MRI sequence and pathologic measurement are shown in **Figure 2**. The 95% limits of difference between HBP and pathologic measurement were −5.2 and 6.8, whereas between TP and pathologic measurement they were −6.2 and 6.4.

In the assessment of inter-reader reliability of size measurement, all six MRI sequences showed excellent agreement (ICC >0.9; **Table 4**). In both readers, HBP showed the highest correlation coefficient (r=0.967 in reader 1 and r=0.958 in reader 2, respectively; **Table 6**), and both TP and HBP demonstrated the lowest absolute difference between MRI and pathologic measurement (2.6 mm on both TP and HBP by reader 1 and 2.2 mm on both TP and HBP by reader2, respectively; **Table 6**). The inter-reader absolute difference of size measurement was 0.9 mm on TP and 0.8 mm on HBP, respectively.

LI-RADS classification

The results of LI-RADS classification according to the size measurement of each MRI sequence are illustrated in **Figure 3**. Of the six MRI sequences, HBP had no LI-RADS category noncategorizable (LR-NC) caused by the lesion invisibility, preventing size measurement. HBP (0.0%, 0/279) showed a significantly lower percentage of LR-NC than T1WI (3.6%, 10/279, p=.024), T2WI (3.9%, 11/279, p=.014), AP (3.2%, 9/279, p=.040), and PVP (3.2%, 9/279, p=.040). Although the percentage of LR-NC was lower on HBP than on TP (1.8%, 5/279), the difference was not statistically significant (p=.380). Regarding LR-3, LR-4, and LR-5, there was no significantly different LI-RADS classification among the six MRI sequences (p≥.122).

Discussion

In the present study, we found that hepatobiliary-phase imaging was superior to all other sequences in respect to both visualization score (mean of 4.1 on a 5-point scale) and correlation with pathologic measurement (r=0.965 and mean absolute difference=2.4 mm). In addition, of the six MRI sequences evaluated, hepatobiliary-phase imaging provided clear LI-RADS classifications without any LR-NC categories. Therefore, hepatobiliary-phase imaging may be the optimal MRI acquisition for measuring hepatic observations on gadoxetate disodium-enhanced MRI.

In our study, HBP showed the highest visualization score for hepatic observations. Unlike the result of Seuss et al., who reported that AP had the highest percentage of visible HCC (96–98%) on extracellular contrast-enhanced MRI, AP did not have a high visualization score in our study (fifth highest of the six MRI sequences). Considering the smaller administered volume and lower gadolinium content of gadoxetate disodium-enhanced MRI in comparison with extracellular contrast-enhanced MRI (13), the weak arterial hyperenhancement with gadoxetate disodium could cause a relatively low visualization score. By contrast, we found that HBP had the highest visualization score, a finding similar to previous studies that reported improved detection and localization of focal hepatic observations, including HCC, using gadoxetate disodium-enhanced MRI(14-16) (e.g., the sensitivity for hypovascular HCC was significantly increased from 59% to 95% using HBP imaging with gadoxetate disodium-enhanced MRI(17)). This good performance can be explained by high lesion-to-liver contrast and high conspicuity during the HBP of gadoxetate disodium-enhanced MRI (18, 19).

The observation sizes on all of the six MRI sequences showed significant strong correlations with those on pathologic assessment (r>0.9; p<.001). This indicates that size measurement on gadoxetate disodium-enhanced MRI is reliable. In particular, the mean absolute difference between MRI and pathologic measurement was 3 mm or smaller on all MRI sequences. Our results showed smaller absolute differences than those of Seuss et al. (2.3–3.0 mm vs. 4.3–6.8 mm). We think this difference may be because we measured the maximal diameter of hepatic observations using both axial and coronal plane MRI, whereas Seuss et al used only axial plane MRI (10).

Both TP and HBP showed lower absolute differences than PVP, which had the lowest absolute difference in a previous study (10). The lesion-to-liver contrast on PVP is determined by the true enhancement or washout of lesions, whereas that on the TP of gadoxetate disodium-enhanced MRI is derived not only from true enhancement and washout of lesions, but also from enhancement of surrounding hepatic parenchyma, because the uptake of gadoxetate disodium by hepatocytes starts approximately 90 s after contrast injection (20). In other words, TP imaging has characteristics of both PVP and HBP imaging, which may be the reason for the better performance of size measurement on TP in comparison with that on PVP. In addition, given the differences in pharmacokinetics between gadoxetate disodium and other extracellular contrast agents, the results for TP in our study should be

interpreted differently to those of the equilibrium-phase in the previous study (10). By contrast, AP and T2WI showed relatively large absolute differences in our study (mean absolute difference = 2.8 mm on AP and 3.0 mm on T2WI). This is in line with the LI-RADS v2018 guidance, which does not recommend measuring the size of observations on AP or DWI if the margins are clearly visible on a different phase. Because reactive or perfusion-related change in peritumoral liver parenchyma is often highly visible on AP imaging and susceptibility artifact or marked anatomic distortions may be encountered on DWI (6), size measurement on these sequences may not be reliable.

Regarding the LI-RADS classification, there was no significant difference in LR-3, LR-4, and LR-5 categorizations among the six MRI sequences. Considering the fact that the mean absolute difference between MRI and pathologic measurement was 3 mm or smaller on all MRI sequences and LI-RADS classification can depend on observation size measurement only in the case on the boundary of size criteria (i.e., an arterial-phase hyperenhancing observation with washout can be categorized into LR-4 when measured as 9 mm, whereas LR-5 when measured as 11 mm, **Figure 5**), the effect of observation size measurement on LI-RADS classification may not be substantial. However, HBP had no LR-NC category because all observations were visible. This has a clinical implication that HBP enables LI-RADS classification by measuring observation size in all cases. Our findings suggest that HBP provides not only accurate size measurement, but also clear LI-RADS classification.

Our study has several limitations. First, a selection bias may have been introduced by the inclusion of only surgically-resected observations, and this may have resulted in the high proportion of HCC in our study. However, to minimize this limitation, we consecutively included all surgically-resected hepatic observations, whether non-HCC malignancies, benign lesions, or HCCs, rather than exclusively including HCCs diagnosed from liver explant, as was performed in a previous study (14). Second, although LI-RADS suggests that observation size is measured on the MRI sequences in which margins are clearest, we measured observation size on the six MRI sequences to determine the optimal MRI sequence in terms of size measurement in comparison with pathologic measurement. In addition, although LI-RADS suggests that an observation can be considered as LR-NC if it cannot be categorized because key phases were omitted or degraded, we categorized the observation into LR-NC when LI-RADS classification was not available because the lesion was invisible, preventing size measurement.

Conclusions

In conclusion, hepatobiliary-phase images had the best lesion visibility and highest correlation of measured observation size with pathologic assessment among the six MRI sequences gadoxetate disodium-enhanced MRI. Furthermore, HBP could provide the clearest LI-RADS classification with the lowest LR-NC percentage. Therefore, hepatobiliary-phase images can be considered clinically

useful for measuring hepatic observations on gadoxetate disodium-enhanced MRI.

Table 1. MRI technique

	Sequence							
	T1 VIBE		Dual-echo T1 GRE		Navigator-triggered TSE T2		DWI[#]	
	1.5-T	3.0-T	1.5-T	3.0-T	1.5-T	3.0-T	1.5-T	3.0-T
Repetition time, *ms*	4.1	4.0	164	125	5208	3940	2000	6200
Echo time, *ms*	1.5	1.9	2.3,OP; 4.6,IP	1.3, OP; 2.6, IP	88	76	81	70
Flip angle, °	10	9	70	70	150	126	90	90
Matrix	320×260	384×250	256×192	320×208	288×384	312×384	192×156	303×379
Field of view	350×284	380×308	350×260	380×308	284×379	308×379	370×240	240×300
Echo train length	NA	NA	NA	NA	13	22	122	44
Section thickness, *mm*	3	3	6	5	6	5	6	5
Intersection gap, *mm*	0	0	1.2	1	1.2	1	1.2	1
No. of signal acquisitions	1	1	1	1	2	2	5	2
Acceleration factor for parallel imaging[*]	2	4	2	2	2	2	2	2

T1, T1-weighted; VIBE, volumetric interpolated breath-hold examination; GRE, gradient-recalled echo; TSE, turbo-spin echo; T2, T2-weighted; DWI, diffusion-weighted imaging; OP, out-of-phase; IP, in-phase; NA, not applicable.

[*]Parallel imaging was performed using a k-space-based technique (GRAPPA at 1.5-T or CAIPIRINHA at 3.0-T; Siemens Healthineers).

[#]Diffusion-weighted imaging was performed using four b-values of 0, 50, 500, and 900 s/mm^2.

Table 2. Baseline characteristics of the patients and lesions

Characteristic	Value
No. of patients	253
Age (y)	63.6 ± 9.4 (39.0–84.0)
Sex	
Male	187 (73.9)
Female	66 (26.1)
Liver cirrhosis	114 (45.1)
Risk factor	
Hepatitis B	203 (80.2)
Hepatitis C	21 (8.3)
Hepatitis B and C	2 (0.8)
Alcoholic liver disease	15 (5.9)
Others	12 (4.7)
No. of lesions	279
Size (mm)	26.4 ± 11.2 (4.0–50.0)
< 10[a]	12 (4.3)
10–19	71 (25.4)
≥ 20[a]	196 (70.3)
Pathology	
HCC	257 (92.1)
Non-HCC	32 (11.5)
Other malignancy	21 (7.5)
Benignity	11 (3.9)

Values are presented as mean ± standard deviation (range) or number (%).

HCC, hepatocellular carcinoma.

[a]Size criteria for LIRADS classification.

Table 3. Comparison of visualization scores between the six MRI sequences

Sequences	Mean ± SD	p-value					
		T1-weighted imaging	T2-weighted imaging	Arterial phase	Portal-venous phase	Transitional phase	Hepatobiliary phase
T1-weighted imaging	3.4 ± 0.8	-	<.001	.021	<.001	<.001	<.001
T2-weighted imaging	3.6 ± 0.8	<.001	-	<.001	<.001	.668	<.001
Arterial phase	3.3 ± 0.8	.021	<.001	-	.028	<.001	<.001
Portal venous phase	3.2 ± 0.8	<.001	<.001	.028	-	<.001	<.001
Transitional phase	3.6 ± 1.1	<.001	.668	<.001	<.001	-	<.001
Hepatobiliary phase	4.1 ± 0.6	<.001	<.001	<.001	<.001	<.001	-

SD, standard deviation.

Table 4. Intraclass correlation coefficients for visualization score and size measurement

Sequence	Visualization score	Size measurement
	ICC (95% CI)	ICC (95% CI)
T1-weighted imaging	0.827 (0.781–0.863)	0.996 (0.994–0.996)
T2-weighted imaging	0.835 (0.791–0.870)	0.996 (0.995–0.997)
Arterial phase	0.780 (0.721–0.826)	0.995 (0.994–0.996)
Portal venous phase	0.817 (0.769–0.856)	0.994 (0.993–0.996)
Transitional phase	0.778 (0.719–0.825)	0.994 (0.993–0.996)
Hepatobiliary phase	0.843 (0.801–0.876)	0.995 (0.993–0.996)

ICC, intraclass correlation coefficient; CI, confidence interval.

Table 5. Correlation coefficients and absolute differences in observation size between imaging and pathologic assessments

Sequence	*r*[a]	Absolute difference (mm)[b]	
		Mean ± SD	Range
T1-weighted imaging	0.954	2.6 ± 2.3	0–13
T2-weighted imaging	0.949	2.9 ± 2.7	0–16
Arterial phase	0.945	2.8 ± 2.7	0–14
Portal venous phase	0.946	2.7 ± 2.6	0–15
Transitional phase	0.960	2.3 ± 2.2	0–12
Hepatobiliary phase	0.965	2.4 ± 2.1	0–11

[a]All correlations were statistically significant ($p<.001$).

[b]Absolute errors were significantly different for transitional phase compared with all sequences ($p<.036$) and hepatobiliary phase compared with all sequences ($p<.028$) except for T1-weighted imaging ($p=.055$). No significant difference was found between transitional phase and hepatobiliary phase ($p=.344$).

Table 6. Correlation coefficients and absolute differences in observation size between imaging and pathologic assessments in the two readers

Sequence	Reader 1		Reader 2		Absolute difference between the two readers (mm)
	r[a]	Absolute difference (mm)	r[a]	Absolute difference (mm)	
T1-weighted imaging	0.956	2.4	0.948	2.8	0.9
T2-weighted imaging	0.949	2.9	0.946	3.1	0.7
Arterial phase	0.946	2.8	0.940	2.9	0.8
Portal venous phase	0.950	2.5	0.937	2.9	0.9
Transitional phase	0.964	2.2	0.951	2.6	0.9
Hepatobiliary phase	0.967	2.2	0.958	2.6	0.8

[a]All correlations were statistically significant ($p<.001$).

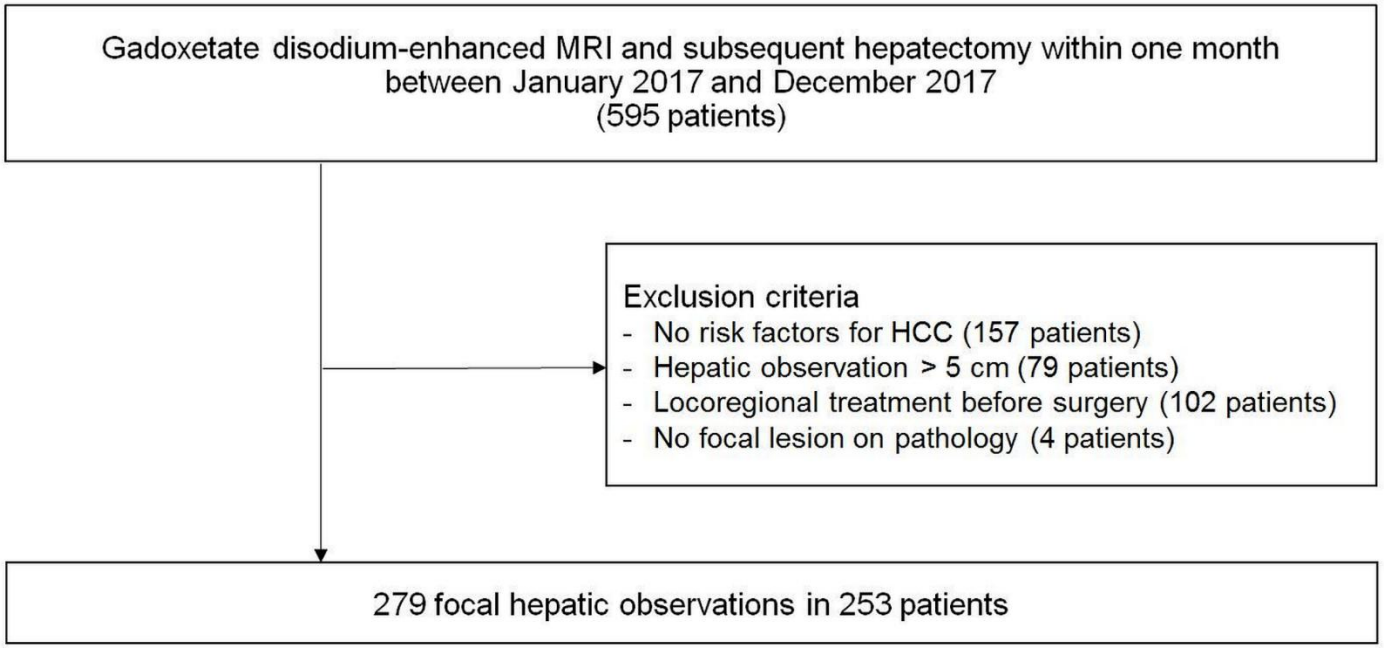

Figure 1. Flowchart of the study population

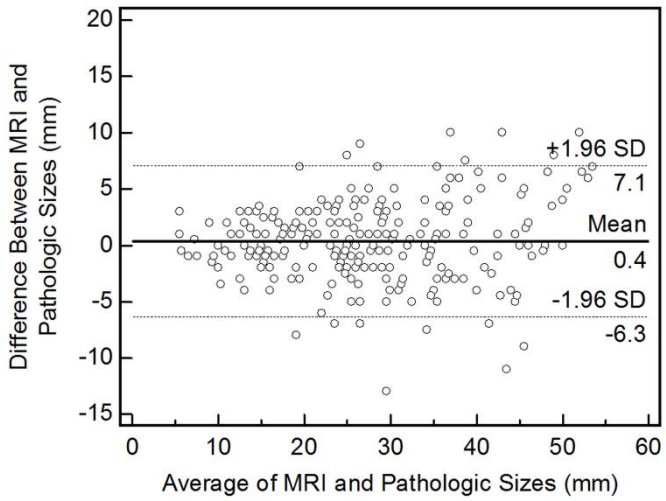

(A) T1-weighted imaging

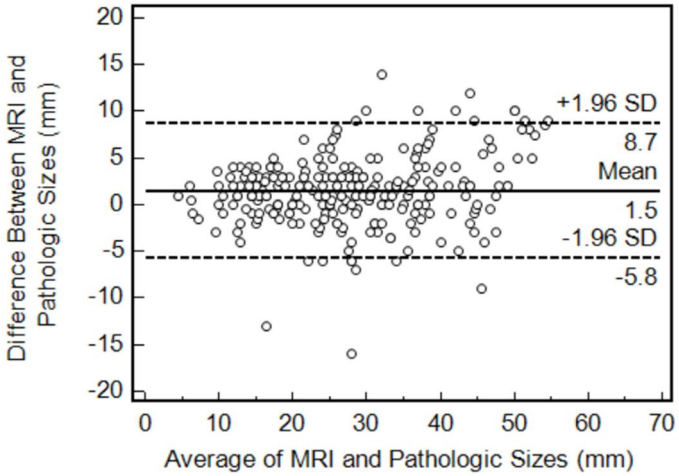

(B) T2-weighted imaging

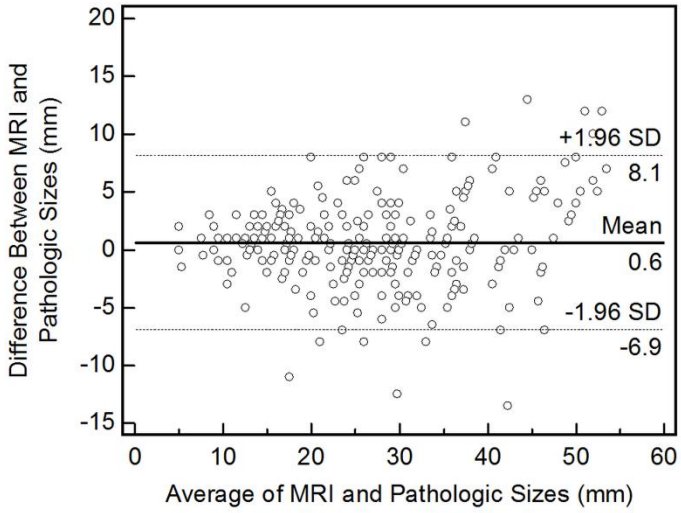

(C) Arterial-phase imaging

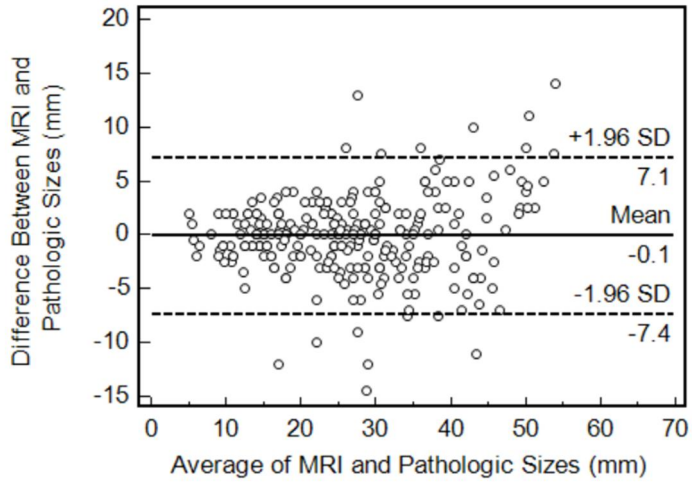

(D) Portal venous-phase imaging

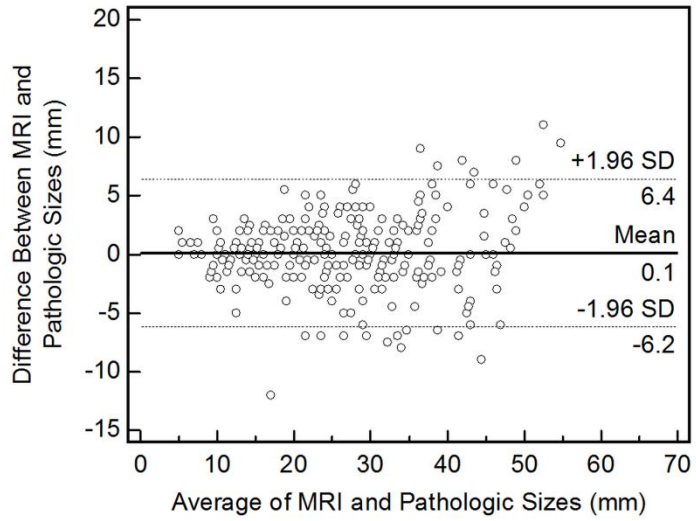

(E) Transitional-phase imaging

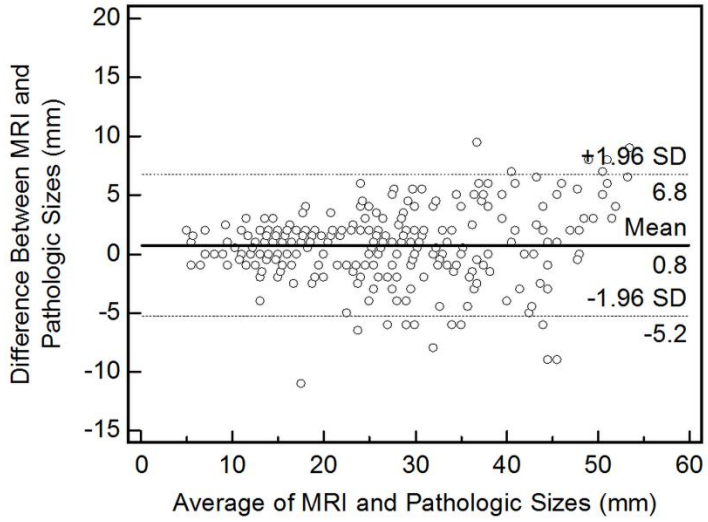

(F) Hepatobiliary-phase imaging

Figure 2. Bland-Altman plots showing agreement between size of hepatic observations on MRI and pathologic measurement

(A) T1-weighted imaging, (B) T2-weighted imaging, (C) arterial-phase imaging, (D) portal venous-phase imaging, (E) transitional-phase imaging, and (F) hepatobiliary-phase imaging. The solid horizontal line represents the mean difference and dashed horizontal lines represent the 95% limits of agreement (defined as 1.96 × standard deviation of differences).

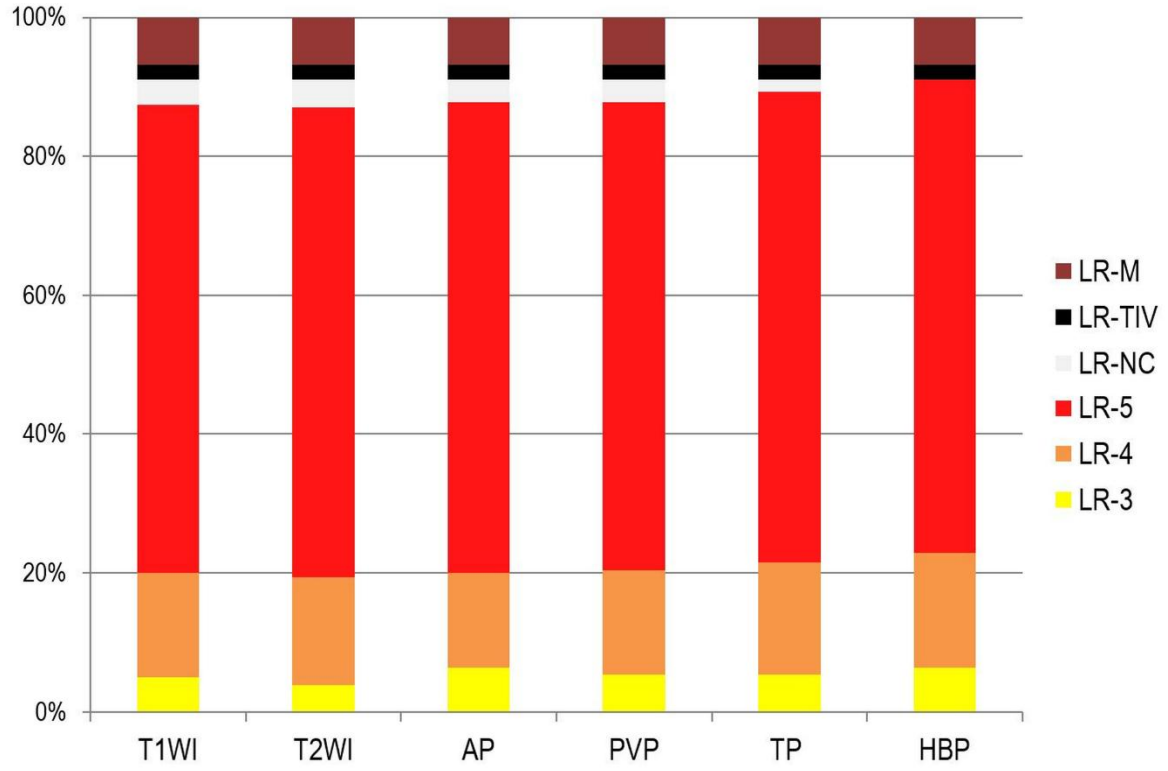

Figure 3. LI-RADS classification according to size measurement of the six MRI sequences

T1WI, T1-weighted image; T2WI, T2-weighted image; AP, arterial-phase; PVP, portal venous-phase; TP. Transitional-phase; HBP, hepatobiliary-phase

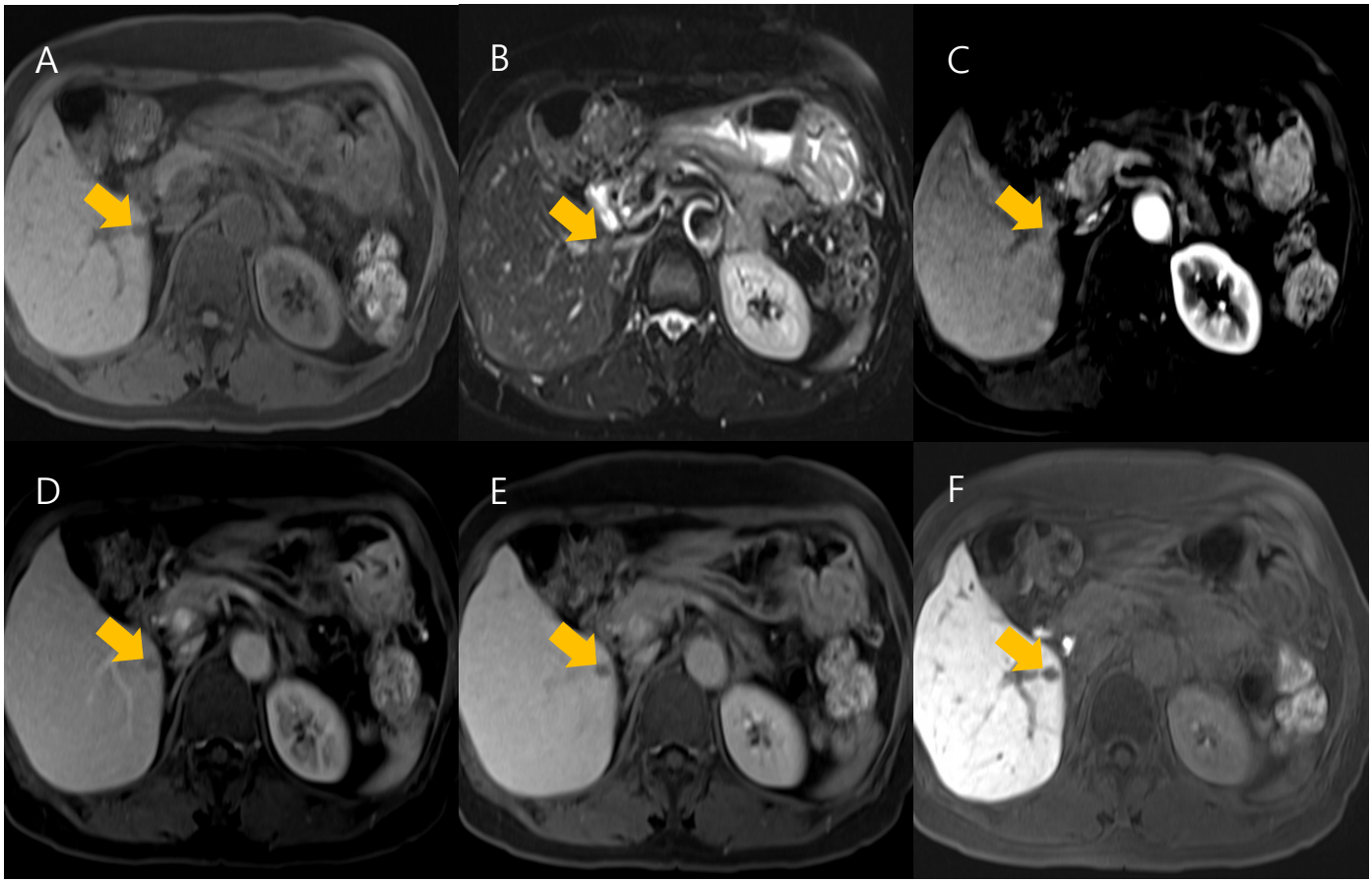

Figure 4. A representative case showing the accurate size measurement in hepatobliary-phase image

(A-F) Gadoxetate disodium-enhanced MRI shows an arterial-phase hyperenhancing lesion in segment VI (C) with washout on PVP (D) and HBP hypointensity (F). It was measured as 9, 8, 10, 8.5, 9, and 11 mm on T1WI (A), T2WI (B), AP (C), PVP (D), TP (E), and HBP (F), which was assigned as LR-4, LR-4, LR-5, LR-4, LR-4, and LR-5, respectively. It was confirmed as HCC and measured as 11 mm on pathologic examination.

References

1. El-Serag HB**.** Hepatocellular carcinoma. N Engl J Med. 2011;365(12):1118-27.
2. Global Burden of Disease Cancer C, Fitzmaurice C, Abate D, et al. Global, Regional, and National Cancer Incidence, Mortality, Years of Life Lost, Years Lived With Disability, and Disability-Adjusted Life-Years for 29 Cancer Groups, 1990 to 2017: A Systematic Analysis for the Global Burden of Disease Study. JAMA Oncol. 2019;5(12):1749-68.
3. European Association for the Study of the Liver. Electronic address eee, European Association for the Study of the L**.** EASL Clinical Practice Guidelines: Management of hepatocellular carcinoma. J Hepatol. 2018;69(1):182-236.
4. Heimbach JK, Kulik LM, Finn RS, et al. AASLD guidelines for the treatment of hepatocellular carcinoma. Hepatology. 2018;67(1):358-80.
5. Radiology ACo;Pages. Accessed at https://www.acr.org/ClinicalResources/Reporting-and-Data-Systems/LI-RADS/LI-RADS1. Accessed August 31, 2021.
6. Radiology ACo;Pages. Accessed at https://www.acr.org/Clinical-Resources/Reporting-and-Data-Systems/LI-RADS/CT-MRI-LI-RADS-v2018. Accessed August 31, 2021.
7. Roncalli M**.** Hepatocellular nodules in cirrhosis: focus on diagnostic criteria on liver biopsy. A Western experience. Liver Transpl. 2004;10(2 Suppl 1):S9-15.
8. Forner A, Vilana R, Ayuso C, et al. Diagnosis of hepatic nodules 20 mm or smaller in cirrhosis: Prospective validation of the noninvasive diagnostic criteria for hepatocellular carcinoma. Hepatology. 2008;47(1):97-104.
9. Huo TI, Wu JC, Lui WY, et al. Reliability of contemporary radiology to measure tumour size of hepatocellular carcinoma in patients undergoing resection: limitations and clinical implications. Scand J Gastroenterol. 2004;39(1):46-52.
10. Seuss CR, Kim MJ, Triolo MJ, et al. Comparison of MRI pulse sequences for prediction of size of hepatocellular carcinoma at explant evaluation. AJR Am J Roentgenol. 2014;203(2):300-5.
11. Mukaka MM**.** Statistics corner: A guide to appropriate use of correlation coefficient in medical research. Malawi Med J. 2012;24(3):69-71.
12. Cicchetti DV**.** The precision of reliability and validity estimates re-visited: distinguishing between clinical and statistical significance of sample size requirements. J Clin Exp Neuropsychol. 2001;23(5):695-700.
13. Huh J, Kim SY, Yeh BM, et al. Troubleshooting Arterial-Phase MR Images of Gadoxetate Disodium-Enhanced Liver. Korean J Radiol. 2015;16(6):1207-15.
14. Sano K, Ichikawa T, Motosugi U, et al. Imaging study of early hepatocellular carcinoma: usefulness of gadoxetic acid-enhanced MR imaging. Radiology. 2011;261(3):834-44.

15. Bashir MR, Gupta RT, Davenport MS, et al. Hepatocellular carcinoma in a North American population: does hepatobiliary MR imaging with Gd-EOB-DTPA improve sensitivity and confidence for diagnosis? J Magn Reson Imaging. 2013;37(2):398-406.
16. Palmucci S**.** Focal liver lesions detection and characterization: The advantages of gadoxetic acid-enhanced liver MRI. World J Hepatol. 2014;6(7):477-85.
17. Inoue T, Kudo M, Komuta M, et al. Assessment of Gd-EOB-DTPA-enhanced MRI for HCC and dysplastic nodules and comparison of detection sensitivity versus MDCT. J Gastroenterol. 2012;47(9):1036-47.
18. Lee YJ, Lee JM, Lee JS, et al. Hepatocellular carcinoma: diagnostic performance of multidetector CT and MR imaging-a systematic review and meta-analysis. Radiology. 2015;275(1):97-109.
19. Choi SH, Byun JH, Kwon HJ, et al. The usefulness of gadoxetic acid-enhanced dynamic magnetic resonance imaging in hepatocellular carcinoma: toward improved staging. Ann Surg Oncol. 2015;22(3):819-25.
20. Tateyama A, Fukukura Y, Takumi K, et al. Gd-EOB-DTPA-enhanced magnetic resonance imaging features of hepatic hemangioma compared with enhanced computed tomography. World J Gastroenterol. 2012;18(43):6269-76.

국문요약

목적: 가도세틱산 조영증강 자기공명영상(MRI)에서 국소 간 병변의 크기를 측정하는 데 있어 병리학적 측정과 비교하여 가장 좋은 영상 시퀀스를 찾고, 간 영상 판독보고 및 데이터 시스템(LI-RADS)에 미치는 임상적 영향에 대해 알아보고자 한다.

연구 재료 및 방법: 가도세틱산 조영증강 MRI를 시행 받고 이어서 간 절제술을 시행 받은 253명의 환자(279개의 병변)가 후향적으로 포함되었다. 두 명의 영상의학과 의사가 독립적으로 6개의 MRI 시퀀스(T1 강조영상, T2 강조영상, 동맥기, 문맥기, 이행기, 간담도기)에서 병변의 가시화 점수와 크기를 측정하였고, 병변의 크기에 따라 LI-RADS 분류를 하였다. 피어슨 상관계수로 MRI에서 측정한 크기와 병리학적으로 측정된 크기의 상관성을 평가하고, 반복측정 분산분석으로 가시화 점수와 MRI와 병리학적 측정 간의 절대적 차이를 비교하였다. 각 MRI 시퀀스에서 측정된 크기에 따른 LI-RADS 분류는 Cochran's Q test를 이용하여 비교하였다.

결과: 279 개의 병변 중 247 개의 간세포암, 21 개의 간세포암이 아닌 악성종양, 11 개의 양성병변이 포함되었다. 6 개의 MRI 시퀀스 중 간담도기가 가장 높은 가시화 점수(4.1 ± 0.6)와 높은 상관계수(r = 0.965)를 보였다. MRI 와 병리학적 측정 간의 절대적인 차이는 이행기에서 가장 낮았으며(2.3 mm ± 2.2), 간담도기에서 다음으로 낮았다(2.4 mm ± 2.1). LI-RADS 분류에서 간담도기에서 분류 불가능(LR-NC)인 경우가 없었다.

결론: 간담도기는 가도세틱산 조영증강 MRI 에서 가시성, 병리학적 소견과의 상관성, LI-RADS 분류를 고려했을 때 국소 간 병변의 크기를 측정하는 데 임상적으로 유용할 것으로 기대된다.